Zhang *et al. Energy Mater* 2021;1:100005
DOI: 10.20517/energymater.2021.07

Energy Materials

Article

Open Access

Check for updates

Enhancing cycle life of nickel-rich $LiNi_{0.9}Co_{0.05}Mn_{0.05}O_2$ via a highly fluorinated electrolyte additive - pentafluoropyridine

Xiaozhen Zhang, Gaopan Liu, Ke Zhou, Tianpeng Jiao, Yue Zou, Qilong Wu, Xunxin Chen, Yong Yang, Jianming Zheng

State Key Laboratory of Physical Chemistry of Solid Surfaces, College of Chemistry and Chemical Engineering, Energy Materials Buliding #5-5307, Xiang'an Campus of Xiamen University, Xiamen 361005, Fujian, China.

Correspondence to: Prof. Jianming Zheng, State Key Laboratory of Physical Chemistry of Solid Surfaces, College of Chemistry and Chemical Engineering, Xiamen University, Xiamen 361005, Fujian, China. E-mail: zhengjm@xmu.edu.cn

How to cite this article: Zhang X, Liu G, Zhou K, Jiao T, Zou Y, Wu Q, Chen X, Yang Y, Zheng J. Enhancing cycle life of nickel-rich $LiNi_{0.9}Co_{0.05}Mn_{0.05}O_2$ via a highly fluorinated electrolyte additive - pentafluoropyridine. *Energy Mater* 2021;1:10005. https://dx.doi.org/10.20517/energymater.2021.07

Received: 7 Sep 2021 **First Decision:** 24 Sep 2021 **Revised:** 1 Oct 2021 **Accepted:** 8 Oct 2021 **First online:** 8 Oct 2021

Academic Editors: Yuping Wu, Hao Liu **Copy Editor:** Yue-Yue Zhang **Production Editor:** Yue-Yue Zhang

Abstract

A highly fluorinated additive, pentafluoropyridine (PFP), is used here to enhance the interfacial stability of the Ni-rich $LiNi_{0.9}Co_{0.05}Mn_{0.05}O_2$ (NCM90) cathode at a cut-off voltage of 4.3 V *vs.* Li/Li^+ at 30 °C. The capacity retention of the NCM90||Li cell is obviously improved from 72.3% to 80.3% after 200 cycles at 1C (1C = 180 mA g^{-1}) when 0.2% PFP is introduced into the baseline electrolyte (1 mol L^{-1} $LiPF_6$ in ethylene carbonate/diethyl carbonate). The improvement in electrochemical performance could be attributed to the formation of a compact and uniform cathode electrolyte interphase (CEI) layer enriched with F-containing polypyridine moieties and LiF species on the NCM90 particles. This CEI prevents side reactions between the electrode and electrolyte and hinders the corrosion of the cathode caused by HF attack. In addition, the formation of internal particle cracks is somewhat suppressed by the robust CEI, thus prohibiting the irreversible phase transformation and better maintaining the superior lithium-ion diffusion kinetics.

Keywords: Pentafluoropyridine, electrolyte additive, cathode electrolyte interphase, $LiNi_{0.9}Co_{0.05}Mn_{0.05}O_2$, lithium-ion batteries

INTRODUCTION

Lithium-ion batteries (LIBs) have been widely investigated and deployed as the power sources of electric vehicles (EVs) owing to their relatively high energy density, long cycle life and environmentally friendliness[1-4]. However, the energy density of LIBs is still not sufficient to achieve EV driving mileages that can compete with conventional cars powered by internal combustion engines, thus impeding the complete substitution of EVs for conventional cars in the automobile market. Consequently, boosting the energy density of LIBs to relieve "range anxiety" has become an urgent requirement that must be met. Ni-rich $LiNi_xCo_yMn_{1-x-y}O_2$ (NCM, $x \geq 0.9$) layered oxides are considered as one of the most promising cathode materials for next-generation LIBs due to their high specific capacity and achievable energy density, in comparison with $LiCoO_2$ and NCM analogues with lower Ni contents[5-7]. However, there still remain key unsolved problems for Ni-rich cathode materials, particularly their rapid capacity deterioration when operated with high charge cut-off voltages of ≥ 4.3 V *vs.* Li/Li^+. The reasons for the rapid capacity deterioration of Ni-rich NCM include the irreversible structural transformation from the layered to the disordered rock-salt phase during the repeat charge/discharge process with excessive lithium utilization[8] and interfacial degradation resulting from the parasitic side reactions between Ni-rich NCM and the electrolyte[9,10].

Structural doping and surface modification are the most commonly adopted measures to improve the structural and interfacial stability of Ni-rich NCM[11-14]. Sim *et al.*[15] coated the surface of $LiNi_{0.9}Co_{0.05}Mn_{0.05}O_2$ (NCM90) particles with 0.5 wt.% tungsten oxide to realize a capacity retention of 84.6% at 1C after 80 cycles, which surpassed the 76.6% achieved for pristine NCM90. Park *et al.*[16] showed that 1 wt.% boron-doped NCM90 could deliver a discharge capacity of 237 mAh g^{-1} at 4.3 V, with an outstanding capacity retention of 91% after 100 cycles at 55 °C, which is 15% higher than for its undoped counterpart. Furthermore, manipulation of the material particle morphology and orientation, as well as the elemental distribution, represents another alternative approach to overcome the degradation[4]. However, these strategies cannot address all the existing issues associated with Ni-rich NCM because the side reactions between the active cathode material and electrolyte cannot be completely prevented.

In this regard, the incorporation of functional additives into the electrolyte is considered a feasible and scalable approach to ameliorate the electrochemical performance of Ni-rich NCM cathodes due to its cost effectiveness. It has been well established that an electrolyte with an appropriate additive can generate a unique and protective cathode electrolyte interphase (CEI) film on the surface of cathode particles during the initial formation process, thus improving the cycling performance of the cell[9,10,17-19]. In particular, research attention has been given to N-containing heterocyclic molecules as functional electrolyte additives due to their unique properties and positive effect in CEI layer formation. For instance, Liao *et al.*[20] utilized a 1-(2-cyanoethyl)pyrrole to construct a protecting CEI film on $LiNi_{0.8}Co_{0.1}Mn_{0.1}O_2$, thereby significantly boosting its cycling performance. Furthermore, extensive research has been conducted in exploiting pyridine derivatives, such as the fluoropyridine family (2-, 3- and 4-fluoropyridine)[21] and 2-vinylpyridine[22]. These additives are able to produce an effective and stable CEI on a $LiMn_2O_4$ cathode and a solid electrolyte interphase (SEI) on a carbon anode. In addition, LiF could be simultaneously formed from the breakdown of fluoropyridine additives to generate a robust LiF-containing CEI layer, which is beneficial for extending the cycle life. However, these additives only contain one fluorine in the molecular structure, which limits the content of LiF in the CEI layer. To date, the effect and functioning mechanism of highly fluorinated pyridines for high energy density Ni-rich NCM remain unknown.

In this work, a highly fluorinated molecule, i.e., pentafluoropyridine (PFP) [Figure 1] is explored for the first time as a functional electrolyte additive to enhance the electrochemical performance of a Ni-rich NCM90 cathode. By introducing 0.2% PFP into the standard electrolyte [1 mol L^{-1} $LiPF_6$ in ethylene

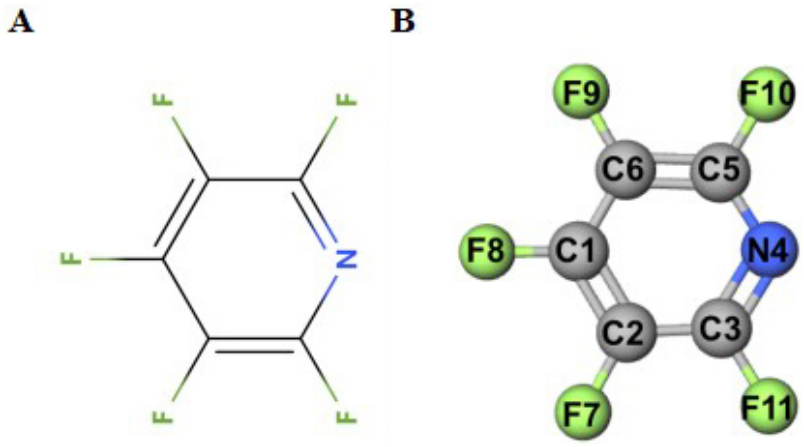

Figure 1. (A) Molecular structure and (B) three-dimensional ball-stick model of PFP. PFP: Pentafluoropyridine.

carbonate(EC)/diethyl carbonate(DEC)], the capacity retention of NCM90 can reach 80.3% after 200 cycles at 1C, which is much higher than that of the standard electrolyte (72.3%). Electrochemical impedance spectroscopy (EIS), transmission electron microscopy (TEM), scanning electron microscopy (SEM) and X-ray photoelectron spectroscopy (XPS) are performed to explore the interfacial chemical environment and microstructural evolution of the NCM90 electrode to obtain deep insights into the essential functioning mechanism for the PFP additive.

EXPERIMENTAL

Calculation method

The highest occupied molecular orbital (HOMO) and lowest unoccupied molecular orbital (LUMO) energies of EC, DEC and PFP with and without solvation with Li^+ ions were calculated on the basis of density functional theory (DFT) with the method of B3LYP in the Gaussian 16 package with the 6-311++G (d, p) basis set[23]. The oxidation potentials of EC, DEC and PFP with and without solvation with Li^+ ions were computed based on Equation (1), where E_{ox} is the calculated oxidation potential of the solvents or additive, $G_{solv}(X)$ and $G_{solv}(X^+)$ are the solvation free energies of molecule X (X = EC, DEC or PFP) and its cation (X^+), respectively, and F is the Faraday constant (96485 C mol^{-1})[24]. The bond dissociation energy (BDE) was calculated to evaluate the strength of the C-F bond and the basis-set superposition error was corrected simultaneously.

$$E_{ox}(V\ vs.\ Li/Li^+)=\frac{G_{solv}(X^+)-G_{solv}(X)}{F}-1.46 \quad (1)$$

Electrode and electrolyte preparation

The single crystalline NCM90 and polycrystalline $LiNi_{0.92}Co_{0.05}Mn_{0.03}O_2$ (P-NCM92) materials were provided by Ningbo Ronbay Technology Co., Ltd. (Ningbo, China) and their basic information is provided in our previous report[10]. To prepare the NCM90 and P-NCM92 electrodes, a slurry containing 80 wt.% active material, 10 wt.% acetylene black as a conductive agent and 10 wt.% poly(vinylidene fluoride) (HSV900, provided by Arkema) as a binder was coated onto Al foil (16 μm in thickness) and then dried at 110 °C in an air-convection oven. After that, the electrode was punched into certain circular disks of 1.54 cm^2 (14 mm in diameter) and baked in a 110 °C vacuum oven for 1 h. The as-prepared electrodes with a loading of 2.5-3.0 mg cm^{-2} were then transferred into an argon-filled glovebox (Shanghai Mikrouna Co., Ltd.) with the moisture and oxygen contents controlled below 0.1 ppm. Lithium metal (15.8 mm in diameter and 2 mm in

thickness from China Energy Lithium Co., Ltd., Tianjin) was used as the negative electrode.

The standard electrolyte (STD) was 1 mol L^{-1} $LiPF_6$ dissolved in EC and DEC (3:7 by weight ratio), as provided by Zhangjiagang Guotai Huarong New Material Co., Ltd. PFP, which was explored as a functional additive, was purchased from Shanghai Bide Pharma Technology Co., Ltd. (Shanghai) and used without further purification. The optimized electrolytes were prepared by adding the PFP additive to the STD with weight percentages of 0.2%, 0.5% and 1.0%, respectively.

Electrochemical measurements

CR2025 coin cells were fabricated with the as-prepared electrodes, Celgard2400 as the separator, Li metal as the negative electrode, along with 100 μL of the electrolyte in the above-mentioned argon-filled glovebox. For long-term cycling performance evaluation, the fabricated coin cells were rested for 5 h at 30 °C and then charged/discharged galvanostatically at 0.1C (1C = 180 mA g^{-1}) for the initial three formation cycles and at 1C charge/1C discharge for the subsequent cycles in the voltage range of 3.0-4.3 V at 30 °C with Neware CT-4008 battery testers. The rate performance was assessed at ascending rates of 0.5C, 1C, 2C, 3C, 5C, 7C and 10C for five cycles, respectively, with the same charging rate of 0.2C after three formation cycles at 0.1C in the voltage range consistent with the long cycling performance test. EIS was performed on CHI760e (Chenhua, Shanghai) with a ±5 mV potential amplitude at the frequency between 100 kHz and 0.001 Hz. Linear sweep voltammetry (LSV) was also recorded on CHI760e at a scanning rate 0.1 mV s^{-1} from the open circuit potential to 7.0 V *vs.* Li/Li^+ at room temperature utilizing a graphite working electrode and lithium metal as the counter and reference electrode.

Characterization

For post-mortem analysis, cycled NCM90 electrodes were obtained from the disassembled cells and then washed by dimethyl carbonate three times to eliminate the residual electrolyte. The morphology of the NCM90 electrodes was characterized by SEM (S-4800, HITACHI). The characterization of CEI layer formation on the NCM90 particle surfaces was carried out by TEM (Tecnai F30 TWIN, FEI). The difference in the chemical components on the surface of the NCM90 electrode was explored by XPS (PHI-5000, ULVAC-PHI) using an Al Kα X-ray (1486.7 eV) source for excitation, with the binding energy referred to residual carbon (C-C) at 284.8 eV.

RESULTS AND DISCUSSION

Oxidative stability of PFP

By means of Gaussian calculations, the HOMO and LUMO energies of EC, DEC and PFP before and after solvation with Li^+ ions were calculated and the results are summarized in Supplementary Table 1. The HOMO energy of PFP molecules solvated with Li^+ ions is determined to be ca. -7.96 eV, in comparison to -9.17 eV for EC and -8.89 eV for DEC, as shown in Figure 2A, indicating that PFP could be oxidized preferentially on the cathode surface. In addition, the LSV curves suggest an onset of current response at ~4.0 V (with a current peak at ca. 4.2 V) when 0.5% PFP is added into the STD, which can be ascribed to the oxidation of PFP, as shown in Figure 2B. This LVS result is in alignment with the theoretical calculation result [Supplementary Table 2] that PFP additive possesses a lower oxidation potential than the EC and DEC solvents. The reduction behavior of PFP was also explored with a SiC working electrode. The differential capacity *vs.* voltage (dQ/dV) curves [Supplementary Figure 1] of the SiC electrode derived from the initial lithiation process show no reduction peak that could be assigned to PFP, which is consistent with the theoretical calculation result.

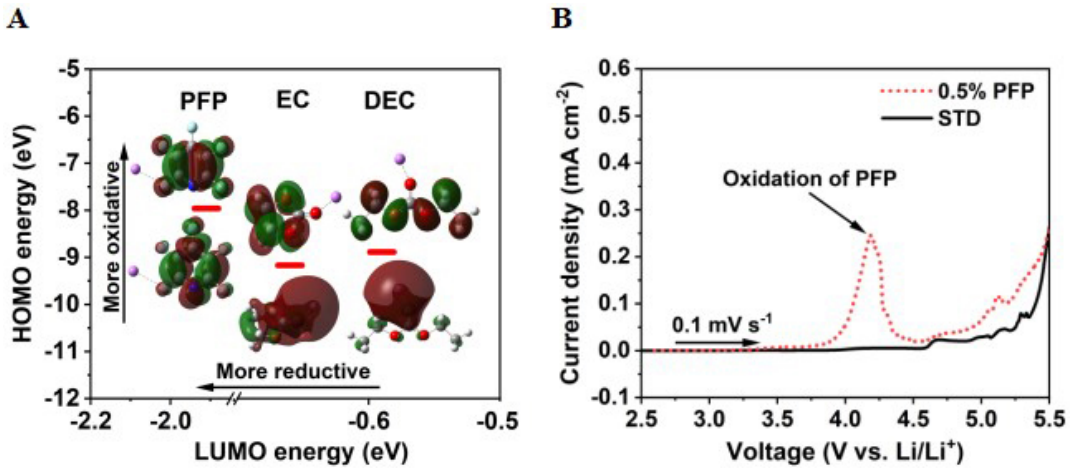

Figure 2. (A) Calculated HOMO/LUMO energies (eV) of EC, DEC, and PFP solvated with Li^+ ions. (B) LSV curves of STD and 0.5% PFP-containing electrolytes measured with a graphite working electrode and Li metal as the counter electrode at a scanning rate of 0.1 mV s^{-1}. Highest occupied molecular orbital; LUMO: lowest occupied molecular orbital; EC: ethylene carbonate; DEC: diethyl carbonate; PFP: pentafluoropyridine; LSV: linear sweep voltammetry; STD: standard electrolyte.

Electrochemical performance of NCM90 and P-NCM92 cathodes in Li half cells

Figure 3A shows the cycling performance of the NCM90 electrode in lithium half cells with STD and electrolytes containing various contents of PFP in the voltage range 3.0-4.3 V at 30 °C. Three formation cycles at 0.1C (1C = 180 mA g^{-1}) were performed before the subsequent cycling under the higher charge/discharge current (1C). The capacity retention of the cell with the STD is found to be only 72.3% after 200 cycles, whereas the capacity retentions of the 0.2%, 0.5% and 1.0% PFP-containing electrolytes are 80.3%, 81.0% and 68.4%, respectively. Careful comparison indicates that the 0.2% PFP-containing electrolyte shows superior electrochemical performance in terms of reversible capacity and capacity retention compared with the other electrolytes.

The initial charge/discharge curves of the cells with and without the PFP additive show that the specific capacity is almost identical for both cells, implying that the PFP additive has no apparent effect on the initial discharge capacity, though with slightly higher electrode polarization at the initial stage of charge, as displayed in Supplementary Figure 2. It is implied that the CEI layer formed on the NCM90 surface may be too thick in the presence of excessive PFP, such as 0.5% or higher, which restricts the movement of Li^+ ions through electrode-electrolyte interface, causing an apparent decrease in the specific capacity at 1C. Furthermore, the average Coulombic efficiency of the cell with the 0.2% PFP-containing electrolyte is 99.6% among 200 cycles, which is higher than the one with the PFP-free electrolyte (99.0%), as shown in Supplementary Figure 3. The positive influence of PFP is further affirmed by the superior cycling stability when the NCM90 electrodes were cycled at higher cut-off voltages of 4.4 and 4.5 V [Supplementary Figures 4 and 5] and when higher active mass loading NCM90 electrodes were evaluated [Supplementary Figure 6].

In addition, compared with the PFP-containing electrolytes, the obvious polarization increase of the charge/discharge plateaus of the cell with the STD during prolonged cycling suggests that the degradation of the electrode-electrolyte interface has a significant effect on cycling performance, as displayed in Figure 3B and C. It is believed that the decomposition of the electrolyte caused by the unwanted parasitic reactions on the NCM90 particle surface contributes to this degradation during cycling. This phenomenon could be further affirmed by the dQ/dV curves [Supplementary Figure 7] during the repeat charge/discharge process, indicating that the cell with the PFP additive exhibits slower shrinkage of the redox peaks at ca. 4.0-4.2 V,

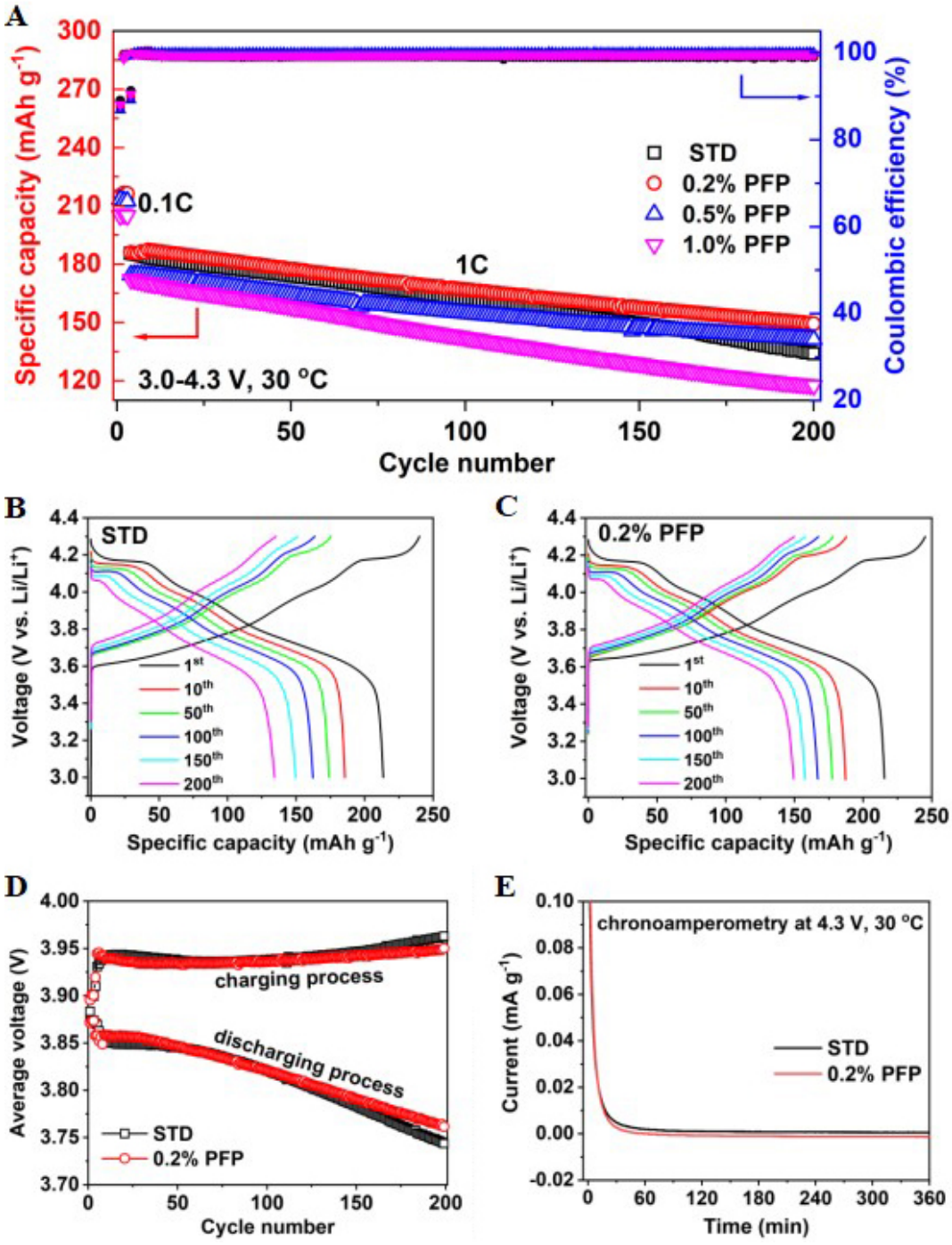

Figure 3. (A) Cycling performance and Coulombic efficiency of NCM90||Li cells with different PFP contents in the voltage range of 3.0-4.3 V at 30 °C. (B, C) Charge/discharge curve evolution of cells (B) without and (C) with PFP. (D) Average charge/discharge voltage during cycling. (E) Chronoamperometry (floating charge at 4.3 V) results of NCM90||Li cells with STD and 0.2% PFP-containing electrolyte. STD: Standard electrolyte; PFP: pentafluoropyridine.

related to the H2-H3 phase transformation[25]. The higher average discharge voltage and lower average charge voltage during the cycling process ascertain the stabilized electrode redox reaction process for the cell with the 0.2% PFP-containing electrolyte, as shown in Figure 3D. In addition, the chronoamperometry

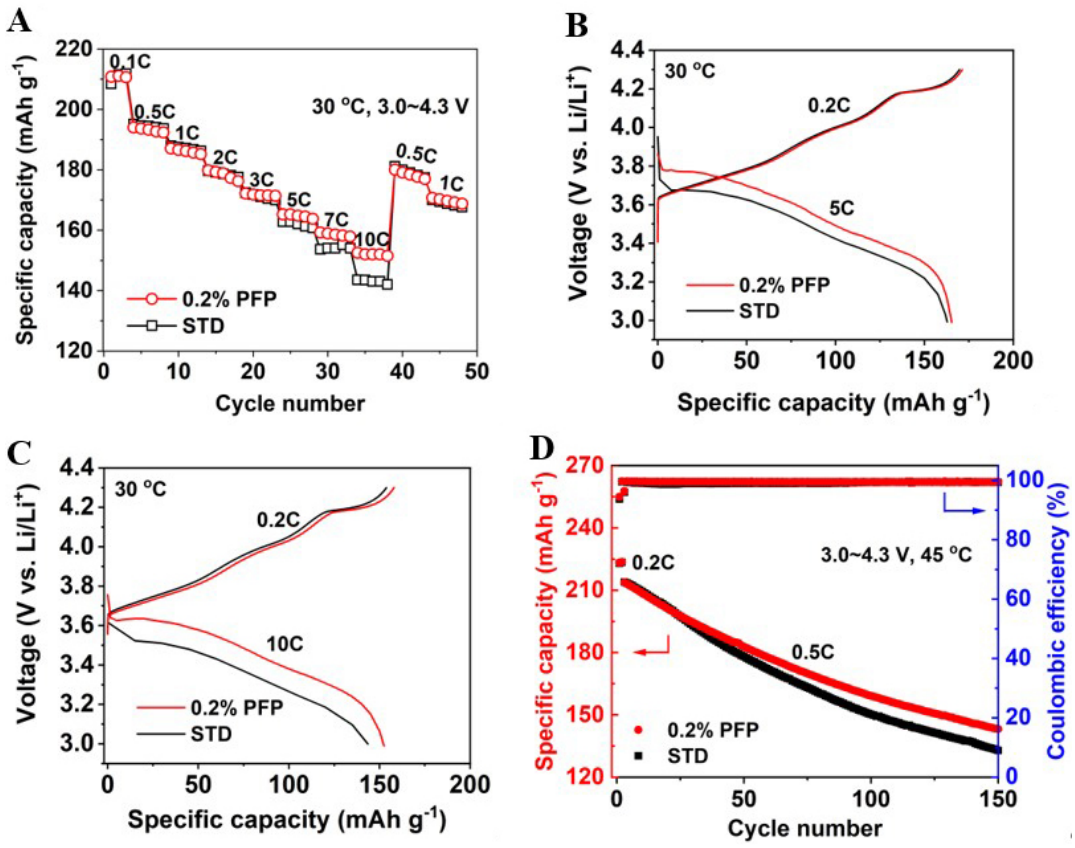

Figure 4. (A) Discharge capacity of NCM90||Li cells at various discharge rates at 30 °C. (B, C) Charge/discharge curves of cells discharging at (B) 5C and (C) 10C rates with and without PFP additive. (D) Cycling performance of P-NCM92||Li cells with STD and 0.2% PFP-containing electrolytes in the voltage range of 3.0-4.3 V at 45 °C. STD: Standard electrolyte; PFP: pentafluoropyridine.

test (i.e., floating charge at 4.3 V) result further evidences the stabilized interfacial CEI as generated with the PFP additive, as reflected by the lower leakage current compared with the one without the PFP additive, as shown in Figure 3E.

Furthermore, the rate performance of the NCM90||Li cells was also investigated at different discharge rates (0.5, 1, 2, 3, 5, 7 and 10C) with the same charge rate of 0.2C in the voltage range of 3.0-4.3 V at 30 °C, as shown in Figure 4A. It is presented that the introduction of 0.2% PFP additive starts to show a positive effect when the discharge rate is above 3C. Interestingly, when the discharge rate is increased (i.e., 5C, 7C and 10C), the discharge capacity of the cell with the PFP-containing electrolyte becomes higher than the cell with the PFP-free electrolyte. Figure 4B and C display the charge and discharge curves of the cell with and without the PFP additive at 5C and 10C rates, respectively. For the cell with the PFP additive, the NCM90 delivers discharge capacities of 165 mAh g^{-1} at 5C and 152 mAh g^{-1} at 10C, well above the discharges in the PFP-free electrolyte (163 mAh g^{-1} at 5C and 143 mAh g^{-1} at 10C). The results indicate that the cell with the PFP additive possesses the capability of fast discharge at high C rates, particularly those above 3C, implying an enhanced NCM90 interface in the presence of the PFP additive.

It is noteworthy that the effectiveness of the PFP additive has also been proved for other Ni-rich cathodes, such as the polycrystalline NCM92 (P-NCM92). Similar to the case for NCM90, with the 0.2% PFP-containing electrolyte, the P-NCM92 electrode shows obviously improved discharge capacities at high C

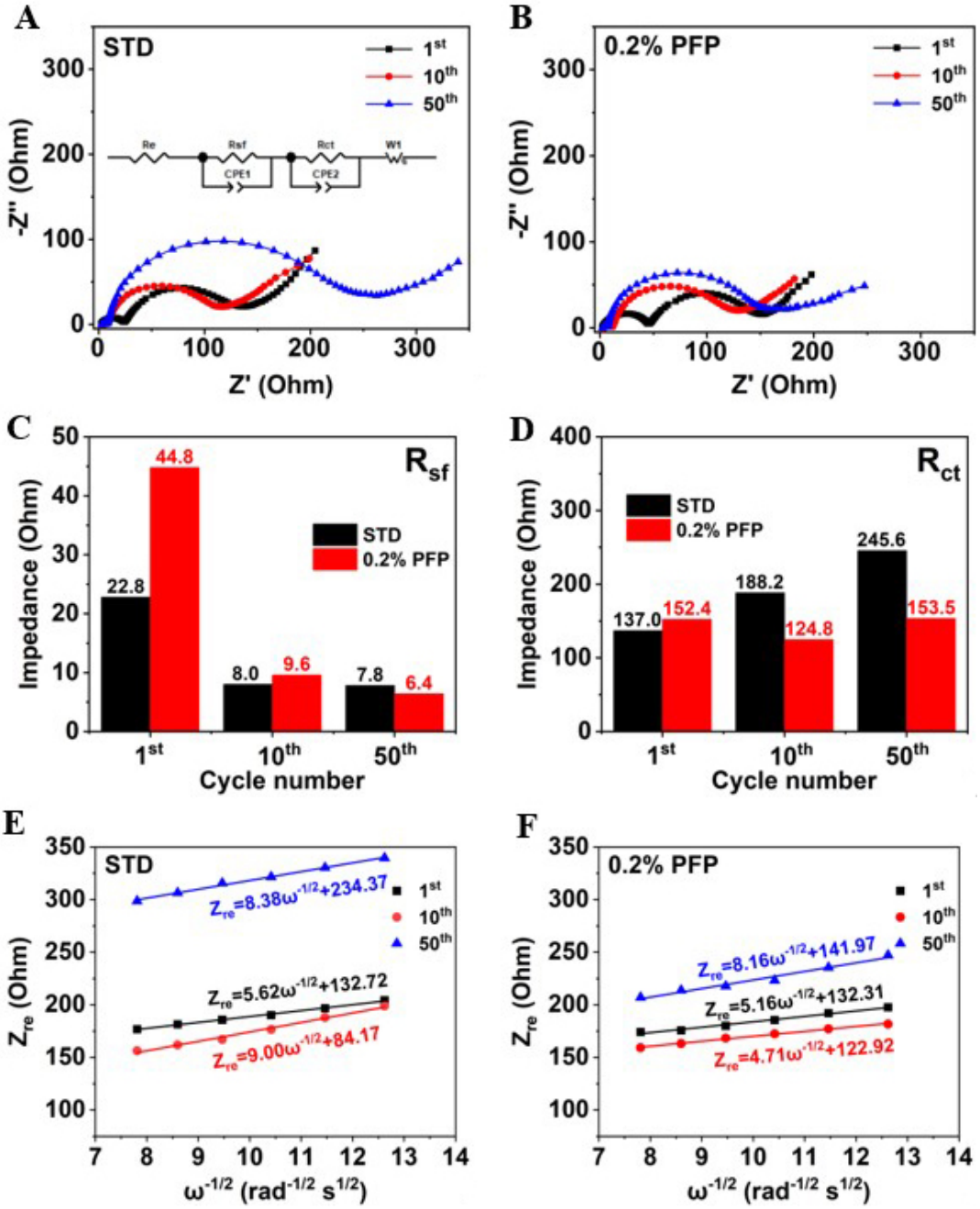

Figure 5. Nyquist plots of NCM90||Li cells at various cycles at room temperature: (A) STD; (B) 0.2% PFP-containing electrolyte. (C, D) Corresponding fitted results of R_{sf} and R_{ct} for NCM90||Li cells. Relationship between Z_{re} and $\omega^{-1/2}$ at low-frequency region for cells with (E) STD and (F) 0.2% PFP-containing electrolyte. STD: Standard electrolyte; PFP: pentafluoropyridine.

rates, as displayed in Supplementary Figure 8. Meanwhile, the high-temperature (45 °C) cycling performance of the P-NCM92||Li cells is also enhanced when introducing PFP into the electrolyte, as shown in Figure 4D. These results suggest that the PFP additive could be broadly applied for promoting the interfacial stability of a wide spectrum of NCM cathodes, depending on the specific demand for practical application.

Kinetics of cathode interfacial film

EIS characterization of the NCM90||Li cells during cycling was carried out to understand the interfacial reaction kinetics and the results are displayed in Figure 5A and B. Two semicircles could be obviously observed at high to medium frequency, which represent the resistance of Li^+ migration through the surface CEI film (R_{sf}) and the charge transfer resistance (R_{ct}). The corresponding fitting results of R_{sf} and R_{ct} are illustrated in Figure 5C and D. It is apparently demonstrated that the R_{sf} [Figure 5C] for the PFP-containing cell (44.8 Ohm) is higher than the STD (22.8 Ohm), which could be contributed to the formation of the protective CEI film on the cathode. After 50 cycles, the R_{ct} [Figure 5D] of the cell with the STD nearly doubles (from 137.0 to 245.6 Ohm) to that of the 1st cycle, while a minimal increase in R_{ct} is observed for the PFP-containing cell (from 152.4 to 153.5 Ohm), suggesting that the PFP-derived CEI helps to maintain lower interfacial resistance and therefore effectively favors the transfer of Li^+ ions through the electrode-electrolyte interface.

It is well established that the slope of EIS spectra at low frequency is associated with the lithium-ion diffusion in the solid electrode (Warburg impedance), which could be used to determine the lithium-ion diffusion coefficients (D_{Li^+}) based on Equations (2) and (3)[26]:

$$Z_{re} = R_{sf} + R_{ct} + \sigma\omega^{-1/2} \quad (2)$$

$$D_{Li^+} = R^2T^2 / (2A^2n^4F^4C^2\sigma^2) \quad (3)$$

where σ represents the Warburg impedance coefficient, ω (ω = 2πf) is the function of frequency (f) for Equations (2) and (3), R is the ideal gas constant (8.314 J mol^{-1} K^{-1}), T is the thermodynamic temperature in K and T = 298.15 K at room temperature, A relates to the surface area of the electrode, *n* is the number of electrons, F is the Faraday constant (96485 C mol^{-1}) and C is the concentration of Li^+ for Equation (3). The relationships between Z_{re} and $\omega^{-1/2}$ in the low-frequency region are presented in Figure 5E and F.

The calculated lithium-ion diffusion coefficients at different cycles are listed in Table 1. For the PFP-containing electrolyte, the lithium-ion diffusion coefficient is higher than that of the STD. In particular, the lithium-ion diffusion coefficient of the NCM90 electrode is identified to be 2.25 × 10^{-10} cm^2 s^{-1} after 50 cycles in the PFP-containing electrolyte, which is higher than that in the STD (2.13 × 10^{-10} cm^2 s^{-1}). These better maintained diffusion kinetics in the presence of PFP additive evidence the enhanced stability of the CEI layer, which prevents the interfacial side reactions and suppresses surface structure degradation.

Interfacial microstructural evolution of NCM90 electrodes

Figure 6A-C present the TEM images of the fresh NCM90 electrode and those cycled in STD and 0.2% PFP-containing electrolytes at 3.0-4.3 V after three formation cycles at 0.1C at 30 °C. As shown in Figure 6A, a smooth surface on the fresh NCM90 cathode can be observed. In comparison, a thick and ununiform interfacial film with a thickness up to ca. 30 nm covers the surface of NCM90 when cycled with STD [Figure 6B], which is unfavorable for the lithium-ion transportation and the interfacial charge transfer reactions[10]. In contrast, in the existence of the PFP additive, a much thinner and compact CEI with a limited thickness of ca. 15 nm can be clearly identified on the surface of NCM90 [Figure 6C]. It is convinced that the improvement of cycling performance was attributed to the thin and compact CEI layer, which could enhance the interfacial structure, restrain unwanted side reactions between electrode and electrolyte and depress the attack by the acidic species (e.g., HF) from the electrolyte.

Table 1. Calculated results of D_{Li}^+ of NCM90||Li cells at different cycles

Cycle No.	STD D_{Li}^+ ($cm^2 s^{-1}$)	0.2% PFP D_{Li}^+ ($cm^2 s^{-1}$)
1st	4.74×10^{-10}	5.62×10^{-10}
10th	1.85×10^{-10}	6.74×10^{-10}
50th	2.13×10^{-10}	2.25×10^{-10}

STD: Standard electrolyte; PFP: pentafluoropyridine.

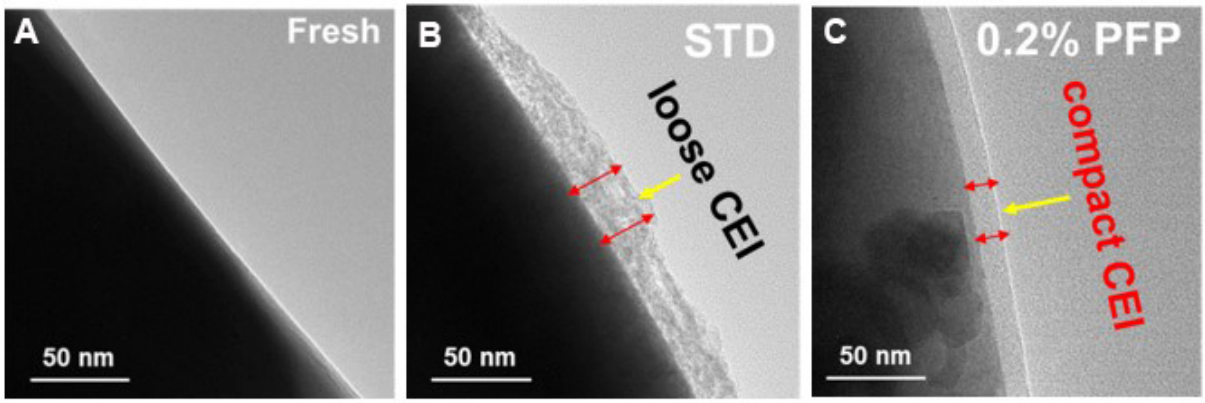

Figure 6. TEM images of (A) fresh NCM90 and the NCM90 cycled in the (B) STD and (C) 0.2% PFP-containing electrolytes after three formation cycles at 0.1C between 3.0 and 4.3 V at 30 °C. TEM: Transmission electron microscopy; STD: standard electrolyte; PFP: pentafluoropyridine.

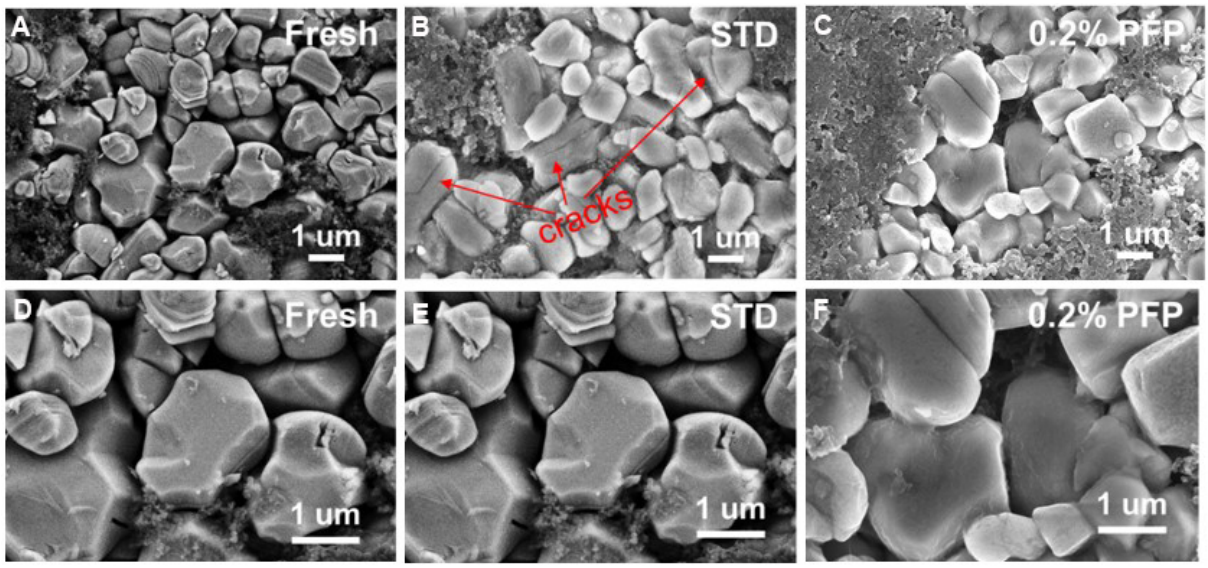

Figure 7. SEM images of (A, D) fresh NCM90 electrode and those cycled in (B, E) STD and (C, F) 0.2% PFP-containing electrolyte after 200 cycles at 1C between 3.0 and 4.3 V at 30 °C. [Magnification: (A-C) 10000×; (D-F) 20000×]. SEM: Scanning electron microscopy; STD: standard electrolyte; PFP: pentafluoropyridine.

SEM characterization was adopted to explore the morphological evolution of the NCM90 particle surface after long-term cycling and the results are shown in Figure 7A-F. The surface of the fresh NCM90 [Figure 7A and D] is smooth and well-defined. However, the surface of the NCM90 electrode particles is

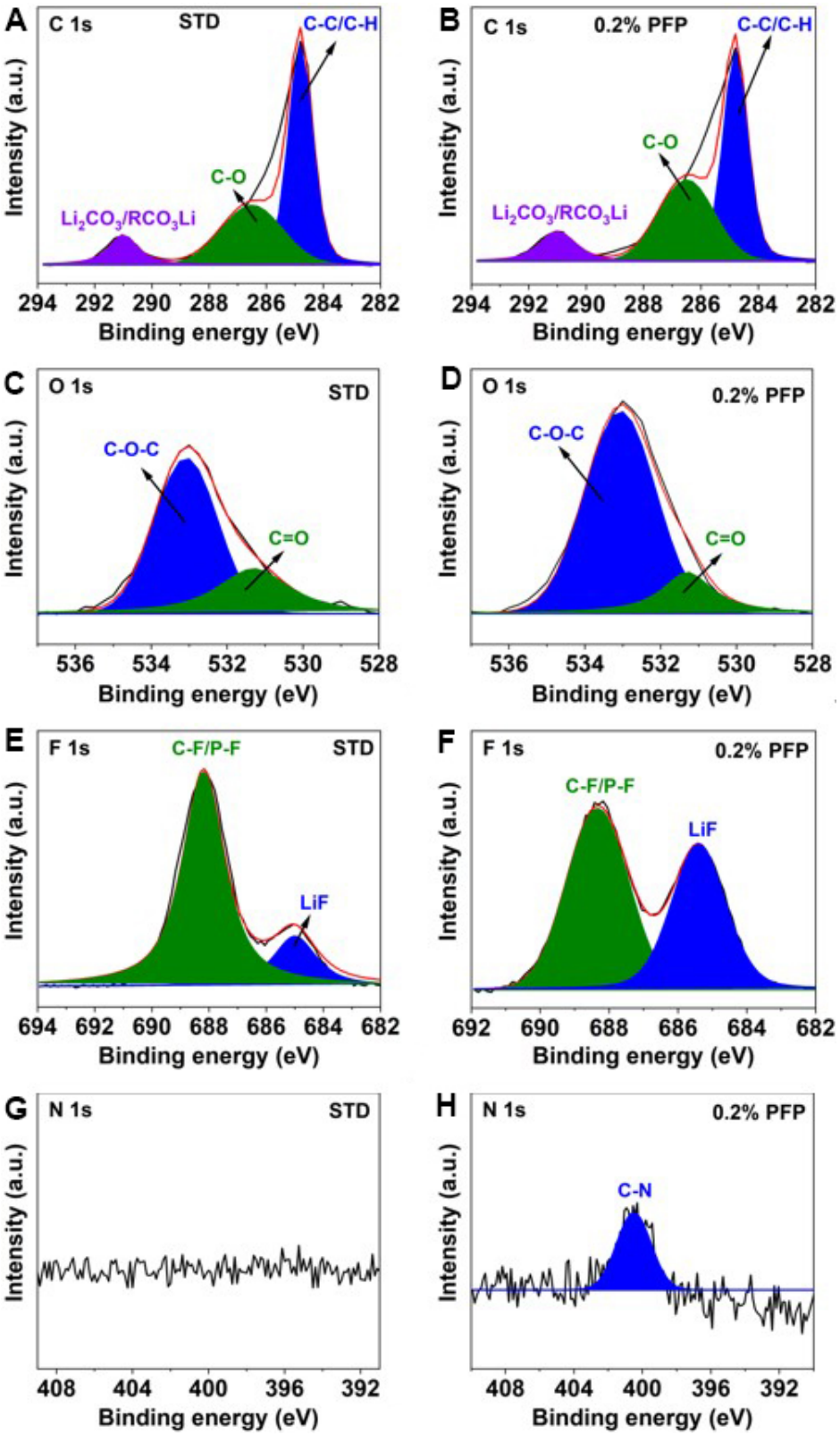

Figure 8. XPS of NCM90 electrodes after three formation cycles at 0.1C with (A, C, E, G) STD and (B, D, F, H) 0.2% PFP-containing electrolyte: (A, B) C 1s spectra; (C, D) O 1s spectra; (E, F) F 1s spectra; (G, H) N 1s spectra. XPS: X-ray photoelectron spectroscopy; PFP: pentafluoropyridine; STD: standard electrolyte.

obviously wrapped with byproducts generated from the decomposition of electrolyte when cycled in the STD [Figure 7B and E]. Slight cracks could also be observed on NCM90 particles for the electrode cycled in the STD (red arrows in Figure 7B), indicating that the particle structure was destructed during cycling, which may result from the HF corrosion and consequent dissolution of transition metal ions. In contrast, the surface of the electrode cycled in the 0.2% PFP-containing electrolyte, as shown in Figure 7C and F, remains smooth and intact, which is analogous to the fresh electrode. This improvement could again be ascribed to the formation of the robust and stable CEI generated in the assistance of the PFP additive, which inhibits the attack of HF species in the electrolyte.

Characterization of CEI chemical composition

In order to better understand the functioning mechanism of PFP on the NCM90 electrode, the chemical components of the surface byproducts were diagnosed by XPS. Figure 8 presents the XPS spectra of the cycled NCM90 cathode harvested from NCM90||Li cells after three formation cycles at 0.1C at a cut-off voltage of 4.3 V. In the C 1s spectra [Figure 8A], a peak appears at 284.8 eV, which can be attributed to C-C/C-H bonds[9]. The peaks centered at 286.5 and 291.0 eV correspond to the existence of C-O bonds and CO_3^{2-} species, respectively[10], which are derived from the decomposition of electrolyte carbonate solvents. The presence of C-O bonds and CO_3^{2-} species is further confirmed in the O 1s spectra [Figure 8C] at 533.0 and 531.3 eV[10], respectively, which could be considered as $ROCO_2Li$ originating from the decomposition of carbonate solvents[27].

In the F 1s spectra [Figure 8E and F], two peaks located at 685.0 and 688.0 eV were observed, which were related to the presence of LiF and C-F/P-F species, respectively[9]. As reported in the literature, LiF is usually identified as one of the major components of the surface film formed at both the cathode and anode surfaces. Nevertheless, there are still disputes regarding the function of LiF, depending on the origin sources of the LiF species, which is typically considered to be formed in two different reaction pathways. Generally, it could be generated by the attack of HF toward the NCM90 electrode surface, which not only devastates the structure of NCM90 cathode but also hinders the lithium-ion diffusion due to its poor conductivity for both electrons and lithium ions, leading to the reduction in the charge-transfer resistance[28-30]. As an alternative pathway, LiF could be produced from the breakdown of the electrolyte additive. The LiF-rich CEI layer as constructed on cathode surface is beneficial for enhancing the interfacial stability against electrolyte attack[21]. In the present study, more LiF is detected on the surface of NCM90 cycled with PFP compared with the one without the PFP additive [Figure 8F]. Based on the superior electrochemical performance with the PFP additive, it is suggested that the LiF could be mainly derived from the preferential oxidation of the highly fluorinated PFP additive, rather than from the attacks by the HF acidic species in the electrolyte.

Comparison of the P 2p spectra in the cycled NCM90 with and without the PFP additive shows that the peak intensity of $Li_xPO_yF_z$ decomposed from $LiPF_6$ is lower in the presence of PFP than that without additive, as illustrated in Supplementary Figure 9A and B. This result further consolidates that the higher LiF peak intensity as detected for the CEI film is generated by the PFP additive other than the decomposition of $LiPF_6$. In the N 1s spectra [Figure 8G and H], the N signal is absent for NCM90 cycled with the PFP-free electrolyte [Figure 8G]. In comparison, there is an obvious N 1s peak located at 400.5 eV found for NCM90 cycled in the PFP-added electrolyte [Figure 8H], which could be attributed to pyridinic nitrogen[21] derived from the PFP additive. The binding energy of the interfacial nitrogen species is higher than that detected for regular pyridinic nitrogen at 398.7 eV[31], which could be explained that a fraction of fluorine atoms are preserved during the electrochemical polymerization of the PFP additive.

Table 2. Calculated BDE results of C-F bonds of PFP molecule

Location of C-F	BDE (kcal mol^{-1})
C2-F7	102.5
C3-F11	103.5
C5-F10	103.5
C1-F8	104.8
C6-F9	104.8

BDE: Bond dissociation energy; PFP: pentafluoropyridine.

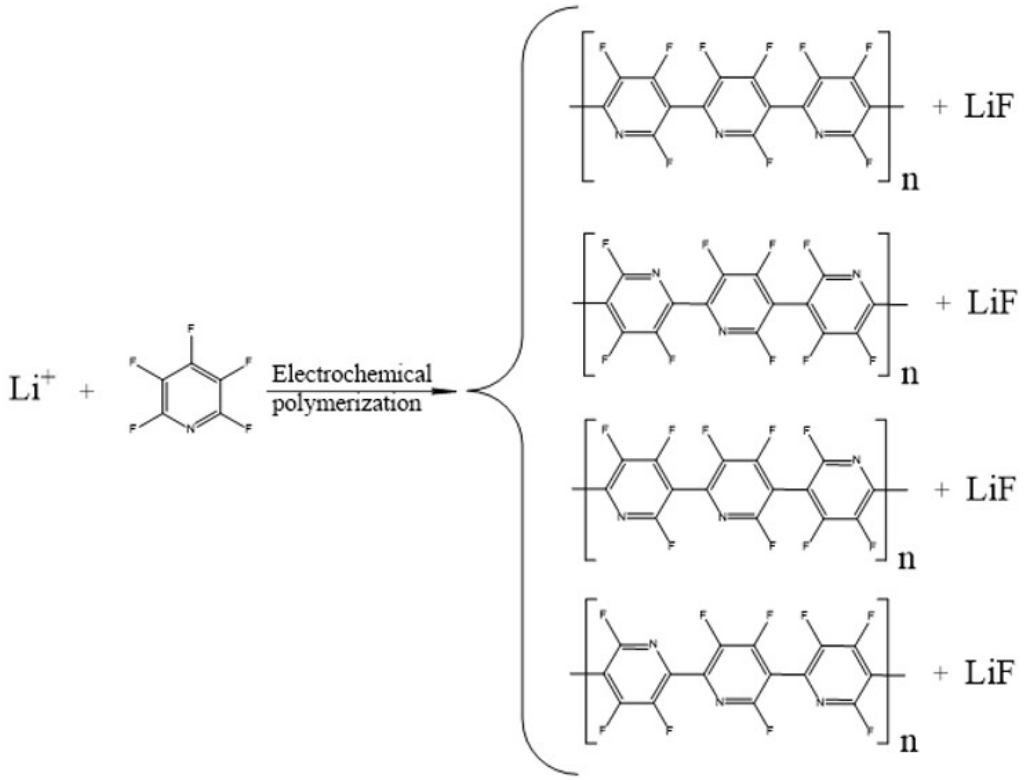

Figure 9. Electrochemical polymerization pathway as proposed for the functioning mechanisms of the PFP additive. PFP: pentafluoropyridine.

Furthermore, to deeply investigate the mechanism for electrochemical performance improvement, the BDE of C-F located at the different position of the pyridine ring were calculated based on DFT, as listed in Table 2. The results show that the fluorine atoms at the C2 position [Figure 1B] possess the lowest BDE, followed by those at the C3 and C5 positions, in the case that one electron is extracted from the PFP molecule. Therefore, the fluorine atoms at C2, C3 and C5 are considered more inclined for electrochemical polymerization, leading to the formation of F-containing polypyridine and LiF, as proposed in Figure 9. Similar electrochemical polymerization mechanism has been previously reported for nitrogen-heterocyclic compounds[20] and pyrimidine derivatives[22].

Finally, the Coulombic efficiency of Li||Cu cells was also studied to explore the effect of PFP on the SEI on the anode surface. The results show that there is no significant distinction of Coulombic efficiency for the cell with and without the PFP additive [Supplementary Figure 10], indicating that the improved

electrochemical performance could be mainly dictated by the enhanced NCM90 interface.

CONCLUSIONS

In this work, a highly fluorinated pyridine PFP has been systematically investigated as a functional electrolyte additive to enhance interfacial stability and electrochemical performance of the Ni-rich NCM90 electrode. It is revealed that the PFP additive could be oxidized prior to the carbonate solvents, forming a compact, uniform and protecting interfacial CEI layer enriched with F-containing polypyridine moieties and LiF species on the NCM90 cathode surface. The enhanced CEI layer could effectively inhibit the electrolyte decomposition and restrain the corrosion on NCM90 electrode by HF species in the electrolyte, giving rise to the improved cycling stability of NCM90 electrode. The development and application of this type of functional electrolyte additive could be beneficial for the industrial application of Ni-rich NCM for developing high energy density LIBs.

DECLARATIONS

Acknowledgments

The authors thank Ningbo Ronbay technology Co., Ltd. and Zhangjiagang Guotai Huarong Co., Ltd. for kindly supplying the cathode material and electrolyte, respectively.

Authors' contributions

Wrote the manuscript: Zhang X, Liu G, Zhou K, Jiao T, Zou Y, Wu Q, Chen X, Yang Y, Zheng J
All authors have given approval to the final version of the manuscript.

Availability of data and materials

The data supporting our findings can be found in the supplementary information.

Financial support and sponsorship

The project was supported by the Xiamen University Nanqiang Yang Talent Program, and the Natural Science Foundation of Fujian Province of China (No. 2020J06004).

Conflicts of interest

All authors declared that there are no conflicts of interest.

Ethical approval and consent to participate

Not applicable.

Consent for publication

Not applicable.

REFERENCES

1. Xia L, Miao H, Zhang C, Chen GZ, Yuan J. Review - recent advances in non-aqueous liquid electrolytes containing fluorinated compounds for high energy density lithium-ion batteries. *Energy Storage Materials* 2021;38:542-70. DOI
2. Wang S, Dai A, Cao Y, et al. Enabling stable and high-rate cycling of a Ni-rich layered oxide cathode for lithium-ion batteries by modification with an artificial Li^+-conducting cathode-electrolyte interphase. *J Mater Chem* ;9:11623-31. DOI
3. Wu F, Liu N, Chen L, et al. Improving the reversibility of the H2-H3 phase transitions for layered Ni-rich oxide cathode towards retarded structural transition and enhanced cycle stability. *Nano Energy* 2019;59:50-7. DOI
4. Sun HH, Ryu H, Kim U, et al. Beyond doping and coating: prospective strategies for stable high-capacity layered Ni-rich cathodes. *ACS Energy Lett* 2020;5:1136-46. DOI
5. Fan Q, Lin K, Yang S, et al. Constructing effective TiO2 nano-coating for high-voltage Ni-rich cathode materials for lithium ion

batteries by precise kinetic control. *J Power Sources* 2020;477:228745. DOI

6. Ye Z, Qiu L, Yang W, et al. Nickel-rich layered cathode materials for lithium-ion batteries. *Chemistry* 2021;27:4249-69. DOI PubMed
7. Liu Y, Fan X, Luo B, et al. Understanding the enhancement effect of boron doping on the electrochemical performance of single-crystalline Ni-rich cathode materials. *J Colloid Interface Sci* 2021;604:776-84. DOI PubMed
8. Zheng J, Yan P, Estevez L, Wang C, Zhang J. Effect of calcination temperature on the electrochemical properties of nickel-rich $LiNi_{0.76}Mn_{0.14}Co_{0.10}O_2$ cathodes for lithium-ion batteries. *Nano Energy* 2018;49:538-48. DOI
9. Liu G, Xu N, Zou Y, et al. Stabilizing Ni-Rich $LiNi_{0.83}Co_{0.12}Mn_{0.05}O_2$ with Cyclopentyl Isocyanate as a novel electrolyte additive. *ACS Appl Mater Interfaces* 2021;13:12069-78. DOI PubMed
10. Zou Y, Zhou K, Liu G, et al. Enhanced cycle life and rate capability of single-crystal, Ni-rich $LiNi_{0.9}Co_{0.05}Mn_{0.05}O_2$ enabled by 1,2,4-1H-triazole additive. *ACS Appl Mater Interfaces* 2021;13:16427-36. DOI PubMed
11. Chen M, Zhang Z, Savilov S, Wang G, Chen Z, Chen Q. Enhanced structurally stable cathodes by surface and grain boundary tailoring of Ni-Rich material with molybdenum trioxide. *J Power Sources* 2020;478:229051. DOI
12. Yan P, Zheng J, Liu J, et al. Tailoring grain boundary structures and chemistry of Ni-rich layered cathodes for enhanced cycle stability of lithium-ion batteries. *Nat Energy* 2018;3:600-5. DOI
13. Yoon M, Dong Y, Hwang J, et al. Reactive boride infusion stabilizes Ni-rich cathodes for lithium-ion batteries. *Nat Energy* 2021;6:362-71. DOI
14. Zhang B, Cheng L, Deng P, et al. Effects of transition metal doping on electrochemical properties of single-crystalline $LiNi_{0.7}Co_{0.1}Mn_{0.2}O_2$ cathode materials for lithium-ion batteries. *J Alloys Compd* 2021;872:159619. DOI
15. Sim S, Lee S, Jin B, Kim H. Effects of lithium tungsten oxide coating on $LiNi_{0.90}Co_{0.05}Mn_{0.05}O_2$ cathode material for lithium-ion batteries. *J Power Sources* 2021;481:229037. DOI
16. Park K, Jung H, Kuo L, Kaghazchi P, Yoon CS, Sun Y. Improved cycling stability of $Li[Ni_{0.90}Co_{0.05}Mn_{0.05}]O_2$through microstructure modification by boron doping for li-ion batteries. *Adv Energy Mater* 2018;8:1801202. DOI
17. Shi C, Shen C, Peng X, et al. A special enabler for boosting cyclic life and rate capability of $LiNi_{0.8}Co_{0.1}Mn_{0.1}O_2$: GReen and simple additive. *Nano Energy* 2019;65:104084. DOI
18. Tan C, Yang J, Pan Q, et al. Optimizing interphase structure to enhance electrochemical performance of high voltage LiNi0.5Mn1.5O4 cathode via anhydride additives. *Chem Eng J* 2021;410:128422. DOI
19. Zhao S, Guo Z, Yan K, et al. Towards high-energy-density lithium-ion batteries: strategies for developing high-capacity lithium-rich cathode materials. *Energy Storage Materials* 2021;34:716-34. DOI
20. Liao B, Hu X, Xu M, et al. Constructing unique cathode interface by manipulating functional groups of electrolyte additive for graphite/$LiNi_{0.6}Co_{0.2}Mn_{0.2}O_2$ cells at high voltage. *J Phys Chem Lett* 2018;9:3434-45. DOI PubMed
21. Xie Z, An X, Wu Z, et al. Fluoropyridine family: bifunction as electrolyte solvent and additive to achieve dendrites-free lithium metal batteries. *J Mater Sci Mater Med* 2021;74:119-27. DOI
22. Komaba S, Itabashi T, Ohtsuka T, et al. Impact of 2-vinylpyridine as electrolyte additive on surface and electrochemistry of graphite for C/$LiMn_2O_4$ Li-ion cells. *J Electrochem Soc* 2005;152:A937. DOI
23. Xing L, Borodin O. Oxidation induced decomposition of ethylene carbonate from DFT calculations-importance of explicitly treating surrounding solvent. *Phys Chem Chem Phys* 2012;14:12838-43. DOI PubMed
24. Leggesse EG, Jiang JC. Theoretical study of the reductive decomposition of ethylene sulfite: a film-forming electrolyte additive in lithium ion batteries. *J Phys Chem A* 2012;116:11025-33. DOI PubMed
25. Noh H, Youn S, Yoon CS, Sun Y. Comparison of the structural and electrochemical properties of layered $Li[NixCoyMnz]O_2$ (x = 1/3, 0.5, 0.6, 0.7, 0.8 and 0.85) cathode material for lithium-ion batteries. *J Power Sources* 2013;233:121-30. DOI
26. Zheng F, Ou X, Pan Q, et al. Nanoscale gadolinium doped ceria (GDC) surface modification of Li-rich layered oxide as a high performance cathode material for lithium ion batteries. *Chem Eng J* 2018;334:497-507. DOI
27. Zheng J, Yan P, Mei D, et al. Highly stable operation of lithium metal batteries enabled by the formation of a transient high-concentration electrolyte layer. *Adv Energy Mater* 2016;6:1502151. DOI
28. Zuo X, Fan C, Liu J, Xiao X, Wu J, Nan J. Lithium tetrafluoroborate as an electrolyte additive to improve the high voltage performance of lithium-ion battery. *J Electrochem Soc* 2013;160:A1199-204. DOI
29. Chen Z, Amine K. Tris(pentafluorophenyl) borane as an additive to improve the power capabilities of lithium-ion batteries. *J Electrochem Soc* 2006;153:A1221. DOI
30. Lee YM, Lee Y, Kang Y, Cho KY. Nature of Tris(pentafluorophenyl)borane as a functional additive and its contribution to high rate performance in lithium-ion secondary battery. *Electrochem Solid-State Lett* 2010;13:A55. DOI
31. Pang Q, Tang J, Huang H, et al. A nitrogen and sulfur dual-doped carbon derived from polyrhodanine@cellulose for advanced lithium-sulfur batteries. *Adv Mater* 2015;27:6021-8. DOI PubMed